Article

What Causes the Arabian Gulf Significant Summer Sea Surface Temperature Warming Trend?

Kamal A. Alawad [1,2,*], **Abdullah M. Al-Subhi** [1], **Mohammed A. Alsaafani** [1] and **Turki M. Alraddadi** [1]

1   Marine Physics Department, Faculty of Marine Sciences, King Abdulaziz University, P.O. Box 80207, Jeddah 21589, Saudi Arabia
2   Weather Forecast Division, Sudan Meteorological Authority, Khartoum 574, Sudan
*   Correspondence: kmohamad0001@stu.kau.edu.sa or kalawad@ersad.gov.sd

Abstract: The present study investigated the significant sea surface temperature (SST) warming trend during the summer season over the Arabian Gulf (AG) and its links with the large-scale atmospheric driver, namely, the Atlantic multidecadal oscillation (AMO), from 1900 to 2021. The link between the AMO and the AGs oceanic circulations has received little scientific attention. It has been found that there is a significant spatial positive trend, with a maximum of up to 0.6 °C per decade over the far northern end, while the time series trend shows a significant shift after 1995, with an average value of about 0.36 °C per decade. The spatial trend in the AG is eight times and four times higher than the global value from 1980 to 2005 using HadISST and OISST, respectively. The AMOs significant role in the AGs SST significant warming trend has been confirmed by the spatial and temporal correlation coefficient, which is above 0.50 and 0.48, respectively, with statistical significance at the 99% level. The underlying mechanisms that explained the AMO-related AGs SST decadal variability can be explained as follows: when the AMO is in a positive phase, the surface northwesterly wind weakens, leading to (1) less advection of the relatively cold air masses from Southern Europe to the AG and surrounding areas, (2) less evaporation, and thus less surface cooling (3); thus, this enhances the water masses stratification and decreases the upwelling process, and vice versa occurs for the negative phase. For the air temperature, the positive AMO phase coincides with the occurrence of warm air masses covering all of the Arabian Peninsula, North Africa, and Southern Europe. These processes prove that the AMO is a possible candidate for the AGs SST decadal variability, hence enabling a better evaluation of future climate scenarios for this important region. Our results provide initial insights into the AMO-driven spatiotemporal variability in the SST over the AG and prove that the relation is nonstationary over time. Further analyses are required to explore whether the impacts of the AMO are extended to other oceanic variables such as evaporation rate, heat transport, etc.

Keywords: optimum interpolation sea surface temperature (SST); SST warming trend; SST shift; Atlantic multidecadal oscillation; Arabian Gulf; nonstationary characteristics

1. Introduction

The gradual increasing trend of sea surface temperature (SST) provides clear evidence of global climate change [1]. The potential adverse impacts of ocean climate change on the marine ecosystem have led to an increase in the attention on the subject globally [2,3]. SST is one of the most important ocean climate factors that affect ocean physics and biology. For example, SST variability directly affects the water level, evaporation, horizontal, and vertical water masses transport, and thus the overall ocean circulations. Furthermore, horizontal and vertical transport affects the nutrient flux and oxygen distribution within the water column, and the frequency and intensity of primary production blooms, which may change the global ocean food chain. According to the Intergovernmental Panel on Climate Change (IPCC), the mean global SST trend computed using a linear trend indicated an increasing tendency during the current century [4]. Warming trends are expected

to continue even if the current amount of greenhouse gas emissions decreases [5]. The vulnerability of the Arabian Gulf (AG) to the SST increasing tendency is highly expected, in which shallow water basins such as the AG may display a larger variation in SST increase compared to deep basins [6]. The AG (Figure 1), our current focus, lies in harsh climate conditions. For instance, surface air temperatures frequently reach 50.0 °C due to the prevailing Shamal winds (hot and dry northwest winds with a 7 to 13 m/s speed) mainly during the summer season [7,8]. The Shamal winds bring dust storms to the Arabian Peninsula, and they may last for several weeks [9] due to an anticyclone condition prevailing over Eastern Europe and North Africa, along with a recession of the monsoon trough [10]. Furthermore, the World Meteorological Organization (WMO) committee officially agreed that the air temperature (54.0 °C), which was recorded on 21 July 2016, at Mitribah, Kuwait, is an extreme value [11].
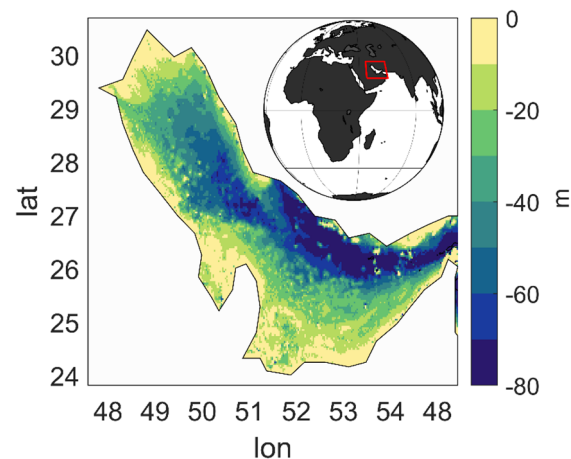

Figure 1. Arabian Gulf (AG) location and bathymetry in (m).

Since the sea surface is the lowest boundary layer of the atmosphere, it is significantly affected by the air temperature. For that, strong correlations were found between air temperature and the SST, especially over the semi-enclosed basin [12]. Due to its physical nature, the AG is considered one of the warmest estuaries worldwide [13,14]. The mean annual SST of 35-year satellite data exceeds 27 °C in the southern part [15], which is associated with a high trend. For example, Al-Rashidi et al. (2009) [16] noted that the northern AG exhibits a significant SST trend of 0.6 °C/decade from 1982 to 2002 using satellite and in situ observations. The same result (0.57 °C/decade) has been observed using extended reconstructed SST (ERSST.v3) during the period of 1950–2010. Although the warming trend was not significant until 1990, it is almost related to the two most recent decades [17], which is about 0.47 °C/decade for the period of 1990–2010 [18]. The most recent study showed that the warming trends reached 0.63 °C/decade [15]. The highest world record extreme SST (37.6 °C) was recorded on 30 July 2020, by in situ stations located in the middle of the Kuwait Bay in the AG, associated with the prevailing southeastern winds (Kous), while above 36 °C was observed in the summer of 2016 and 2017 [19]. In addition, Burt et al. (2019) [20] detected 37.7 °C, but this was on a coral island on the coast of the United Arab Emirates.

Despite the fact that AG corals have been characterized by the highest bleaching thresholds, associated with a superior thermal tolerance compared with other corals worldwide [1], several widespread coral bleaching events have occurred. Previous studies have suggested that El Nino–southern oscillation (ENSO) and the Indian Ocean dipole (IOD) are the possible drivers of oceanic and atmospheric teleconnections [21]. However, one bleaching event (1998) occurred during a positive ENSO year [22], while some others (e.g., 1996, 2010) occurred during negative ENSO years [1,23], suggesting that other drivers are involved.

At this stage, it is important to state that in Al-Rashidi et al.'s study (2009) [16], the contribution of the large-scale driver of the AGs SST warming trend over the northern AG was found to be 60% (0.3 out of 0.5 °C/decade), while the regional drivers were 40%. Furthermore, recent studies have found that the AMO has a strong effect on the Red Sea's SST [24,25], as well as the summer surface air temperature surrounding the AG [26]. The link between the AMO and the AGs oceanic circulations has received little scientific attention. The only paper on this topic used the first mode of empirical orthogonal function analysis, that explains 73% of the total variances, and found that the SST variability over the AG could be attributed to atmospheric changes driven by the AMO, as well as ENSO and IOD, using a 39-year study period [27].

The above findings have motivated us to study one of the large-scale atmospheric drivers, namely, the Atlantic multidecadal oscillation (AMO), which is hypothesized to have a large effect on the AGs SST during the summer season, by highlighting how the signal transferred to the AG, which has not been covered before, using a longer study period (1900–2021). We chose the summer season for three reasons. First, the correlation between the summer and annual SST is 0.90, meaning that it is the main contributor to annual variability. Second, the highest world record extreme SST was recorded in the summer of 2020, while temperatures above 36 °C were observed in the summer of 2016 and 2017. Third, a previous study has proven that in the summer season, the Red Sea's SST, as well as the surface air temperature surrounding the AG, has been impacted by the AMO.

2. Materials and Methods

2.1. Data

We examined the HadISST dataset, which is a global monthly mean SST analysis on a 1° × 1° grid that covers the period of 1900–2021 [28]. Based on in situ sea surface observations combined with satellite-derived estimates of the sea surface data from the post-1985 period, the Hadley Centre for Climate Prediction and Research–UK Met Office provided the HadISST dataset. The Optimum Interpolation SST version 2 (OISST.v2, also known as Reynolds' SST) data for the period 1982–2018 [29] were used in this study. These data were gratefully obtained from the NOAA database in a monthly mean time-scale and with 0.25° × 0.25° resolution grid points. OISST merge different input data sources (satellite and available ships and buoys) irregularly distributed in space and time; then, optimum interpolation methods are applied to fill the spatial and temporal missing values.

The monthly mean U-wind component on the surface and the air temperature on the surface and 850 hpa are derived from the fifth-generation ERA5, European Center for Medium-Range Weather Forecast (ECMWF). ERA5 are reanalysis data assimilating as many observations as possible across the world, combined with a model output to produce global regular grid points. The data we used here are in a monthly mean format, with 0.5° × 0.5° resolution grid points from 1900 to 2021.

2.2. Methodology

The AMO is a large-scale climate mode, occurring on multi-decadal temporal scales [30], and is defined as the annual averaged SST anomaly in the North Atlantic Ocean (0° to 60° N, 0° to 70° W). The positive AMO phase refers to positive SST anomalies over most of the basin, while vice versa occurs for the negative phase.

The main statistical tools used are composite, trend, and linear correlation analyses. Composite analysis was used to derive the anomalies of the SST and the different atmospheric variables of the two periods. The first period is from 1971 to 1996 and the second period (P2) is from 1997 to 2021. Those periods are considered to have a different atmospheric circulation related to the AMO. The reference climatology to generate the anomalies is computed for the whole period of 1971–2021.

The AGs SST trend has been computed using the Mann–Kendall Tau method in each grid point, with a 95% confidence level [31,32]. This non-parametric technique

is widely applied to all types of distributions, i.e., the data do not need to meet any normality assumptions.

A Pearson linear correlation was applied to investigate the relationship between the AMO time series and the AGs SST as well as the atmospheric circulations. The whole analysis is based on the mean of the boreal summer season by averaging the June, July, and August months for all of the data.

3. Results and Discussions

The temporal SST variability in the AG is presented using two datasets with different periods and spatial resolutions by comparing the very long reconstructed SST (HadISST) with the relatively short satellite era (OISST) (Figure 2). It is important to mention that the AGs SST did not always follow the same pattern of the AMO (1930–1965), suggesting that the AGs SST derived from other large-scale climate modes during this period. This is a well-known property and has been known as the nonstationary signals of a large-scale climate, including the AMO, in driving all oceanic and atmospheric circulations [33]. A very long-term dataset identified the nonstationarity in the internal AMO signals from 1650 to 2012, detected by Erkyihun et al. (2005) [34]. Comparable results of a nonstationary relationship throughout the last century between the coral oxygen isotope and ENSO were reported over Kenya [34] and the central Indian Ocean [35]. Clear evidence of nonstationary has been observed over the Red Sea. In Figure 2, Monica et al. (2014) [36] showed that the correlation value between the ENSO and coral oxygen isotope decreased from −0.60 from 1930 to 1960 to −0.08 from 1961 to 1995 during the winter season. The atmospheric circulations patterns indicate that pre-1960 was characterized by anomalies reminiscent of ENSO features, while post-1960 is characterized by anomalies and a phase of East Asian winter monsoons that is independent of the ENSO but closely related to the Siberian anticyclone [36].
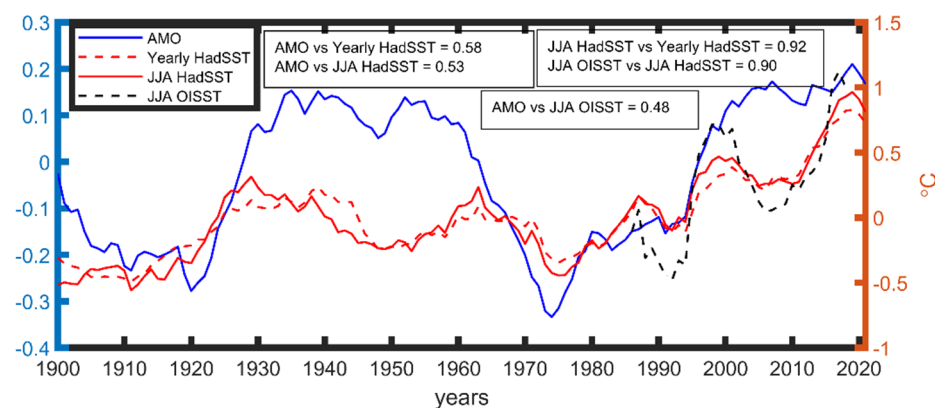

Figure 2. Time series of annual SST (dot red line), summer (solid red line), Atlantic multidecadal oscillation (AMO) (solid blue line) during 1900–2020, and OISST (dot black line) during 1982–2020, and their associated correlation analysis.

It is clear from the temporal variability that the time series of the summer SST is closely related to the annual variability (CC of 0.92, while the CC for the winter SST with that of the annual is 0.6), meaning that the summer season has the dominant signal and can be used to represent this study, as we will proceed to do so in the Section 3. Furthermore, both the annual and summer SST time series are well correlated with the AMO (0.58 and 0.53, respectively), while the correlation of the winter SST with the AMO shows a reasonable value of 0.44.

The observed summer means of the SST satellite era in the AG, averaged over 1971–2021, show a relatively strong meridional gradient, with a 4 °C range over a 600 km distance, compared to the neighbors' semi-enclosed sea. The Red Sea has a 6 °C range over

a 1500 km distance [37]. The AGs SST varies from ∼29 °C on the extreme northern side to ∼33 °C along the southwest United Arab Emirates coast in the south (Figure 3).
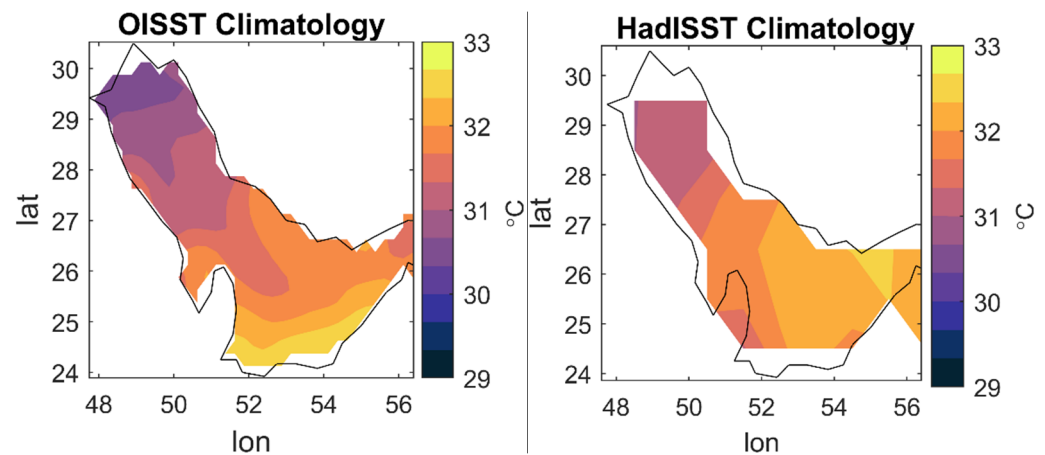

Figure 3. Summer climatology of the OISST and HadISST (1982–2018).

Although the values of the SST vary between the OISST and HadISST (Figure 3), which mainly reflects the limited spatial coverage of the coarse resolution HadISST, they are generally consistent in terms of interannual variability, patterns, and trends.

The low temperature in the north is a natural response to the blowing of northerly surface wind, which brings relatively cold air masses to the area. In addition, the low bathymetry over the north part combined with low solar forcing may be considered possible reasons as to why there was a decrease over the area. While the possible reasons for the high temperature in the southern part are the increasing solar forcing closest to the equator, the vicinity to the Rub Al-Khali desert, and the entrance of relatively warm freshwater from the North Indian Ocean through the Gulf of Oman [15]. Globally, the SST has a higher range over shallow water basins [38].

Figure 4 shows the spatial composite difference in the AGs SST between pre- and post-1996 for HadISST datasets. The AG exhibited a uniform and remarkable warming pattern with more than 0.6 °C, especially over the southern half (Figure 4). The same result has been reflected using OISST but with a higher magnitude, while the entire AG area increased by more than 1 °C (Supplementary). Interestingly, the area-weighted highest OISST increased over the northwestern side, which was characterized by shallow bathymetry. Previous studies have shown that the basins that have shallow water and/or are surrounded by industrial agglomerations (oil and gas), such as the AG, may display a warming pattern larger than the global rate [6]. In addition, the highest warming rate was observed over the relatively cold temperature in the basin. This finding encourages us to provide more attention to atmospheric forcing on the SST in the following analysis since this area is affected by the relatively cold northerly wind from Southern Europe.

In Figure 5, we present the spatial trend analysis in each grid point for the entire study period. The black dot indicates that the trend is significant at 95%. Visually, the trend pattern is similar to the SST difference between pre- and post-1996, as presented in Figure 4. The result shows significant variability towards a positive trend, with a maximum of up to 0.4 °C per decade. The OISST dataset reflects a higher trend value of up to 0.6 °C per decade (Supplementary). It is important to mention that the global SST warming trend is about 0.11 °C per decade based on the 1980–2005 time average [4], meaning that the spatial AG trend is much higher than the global value.

The current analysis supports the previous finding of Al-Subhi, (2019) [15] and Al-Rashidi et al. (2009) [16], who noted a value of approximately 0.6 °C per decade from 1982 to 2016 and 1950 to 2010, respectively, while a value of 0.57 °C per decade was observed by Shirvani et al. (2015) [17]. Regionally, Shaltout and Omstedt, (2014) [39] and Alawad et al. (2020) [25] reported a closer rate over the Western Mediterranean Sea (0.42 °C

per decade) and the Northern Red Sea (0.4 °C per decade), respectively. Recently, many studies have indicated that there were shifts in both the SST and surface air temperature on a decadal time scale in this period. This shift reveals a non-uniform warming trend over the wide area [35–37].
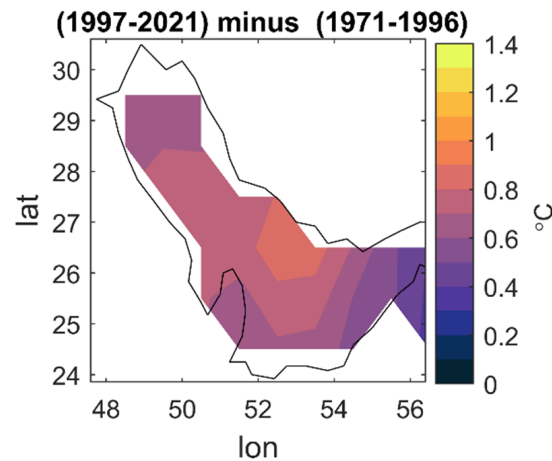

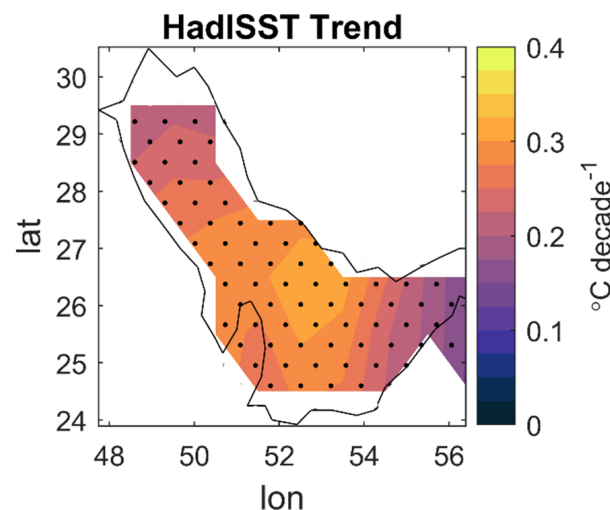**Figure 4.** The SST difference between pre- and post-1996.

Figure 5. The spatial HadISST trend in °C decade^{-1} during the summer season. The dot area indicates the significant area at 95%.

The broader region surrounding the AG has recently been known to be directly affected by the AMO [25,26,40–43]. The manifestation of its relationship within the AG itself can easily be detected by the correlation. Figure 6 shows the spatial correlation of the AMO HadISST datasets. All the results are significant at a 95% confidence level. The spatial correlation has also been explored to reveal the different meridionally responses as the shape of the study area.

The AMO widely modulates the AGs SST through a strong significant relation with an up to 0.50 correlation value (Figure 6). The same analysis using the long-term OISST dataset showed a stronger correlation but with a different pattern, while the northern area, which is close to the North Atlantic, received a stronger AMO signal (Supplementary).

It is not surprising to find that the AMO signal reached the AGs SST; a recent study indicated that the summer surface air temperature surrounding the AG is strongly affected by the AMO [26].
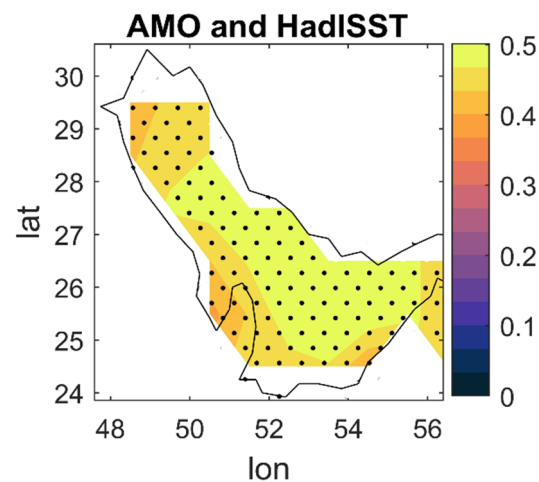
Figure 6. The spatial correlation between the AMO time series and SST. The dot area indicates the significant area at 95%.

Atmospheric Circulations Patterns

One possible cause of the SST increase is a decrease in the surface Shamal wind. Thus, the question arises of to what extent does the AMO force the AGs SST through the Shamal wind over this area? To answer the question, the difference in the Shamal wind before and after 1996 has been investigated, followed by its correlation with the AMO time series and, lastly, the AGs SST. The anomalous Shamal wind is slightly downward over the entire AG by up to −0.6 m/s (Figure 7a). The correlation of the Shamal wind with the AMO shows a negative result (up to −0.5) spread over the same the Shamal wind difference in Figure 7a and the AGs surrounding area. In addition, the AGs SST time series is also negatively correlated with the Shamal wind (Figure 7c). Recent studies have indicated that the Shamal wind is forced by a horizontal pressure gradient between the high-pressure system over the Eastern Mediterranean Sea and the low-pressure system over Iran, Pakistan, and Afghanistan [9,44].

According to previous studies, this result can explain the SST increase from three points of view. First, a decrease in the Shamal wind that blows from the north leads to less advection of relatively cold air masses from Southern Europe [44]. Second, a decrease in the Shamal wind leads to less evaporation and thus less surface cooling process, which leads to an additional decrease in the surface wind speed. Third, a decrease in the Shamal wind enhances the water masses stratification and decreases the upwelling process, especially over shallow basins such as the AG. This process is called the wind speed–evaporation–SST feedback, through the thermodynamic interaction between the atmosphere and surface ocean, and vice versa [45]. Further analyses are required to explore whether the impacts of the AMO are extended to other oceanic variables such as evaporation rate, heat transport, etc.

The AMO has an internal variability in a cycle of around 65–80 years, and it has been turned into a positive phase since the mid-1990s [25,40,41].

The above results indicate that during positive AMO events, the surface Shamal winds reduced, and the AGs SST increased. Therefore, the analysis emphasizes a clear link between the AMO and AGs summer SST increase through the decrease in the Shamal wind.

The physical connection between the AMO and AGs SST can also be investigated throughout a surface (Figure 8) and upper-air temperature at 850 hpa (Figure 9). The vertical temperature advection is a well-known topic relevant to inducing a change in surface temperatures in both the air and ocean [40]. First, the surface and 850 hpa temperature difference before and after 1996 was computed, and it is shown in Figures 8a and 9a, respectively. Their anomalous temperature was upward over a wide area extended from Southern Europe and Northern Africa, including the Red Sea, and covers all Gulf countries.
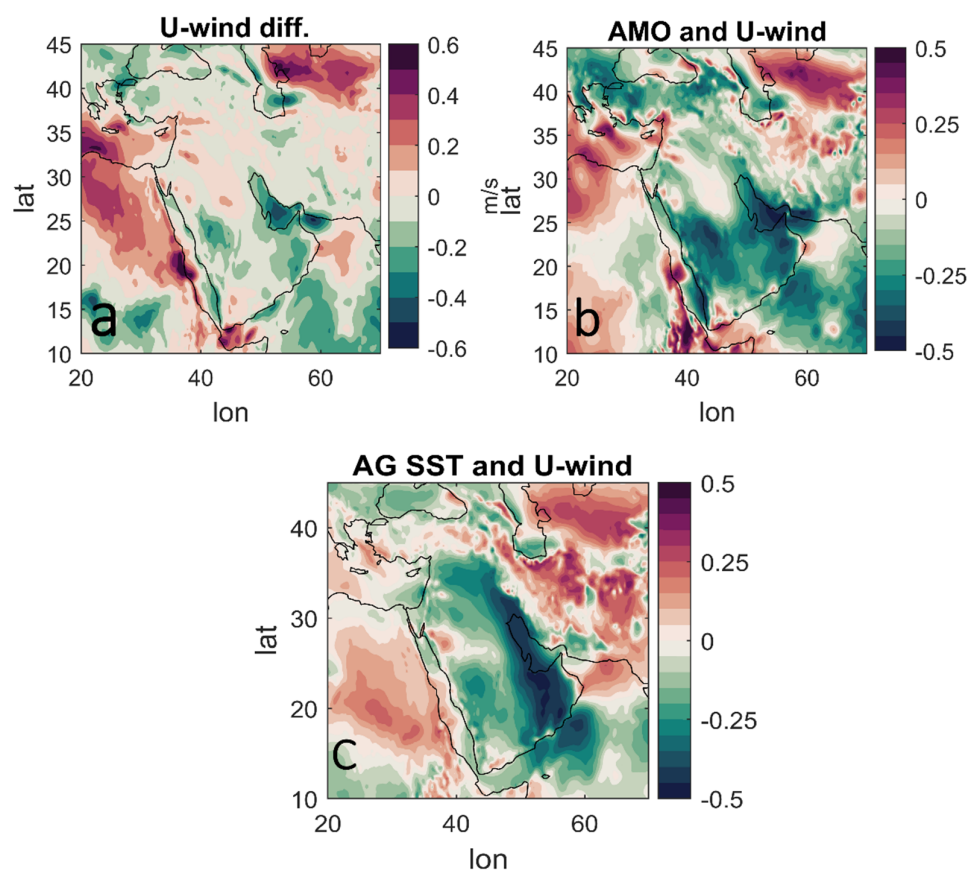
Figure 7. The difference in the U-wind component between pre- and post-1996 (**a**), correlation analysis between the AMO time series and U-wind (**b**), and correlation analysis between the AGs SST time series and U-wind (**c**). All the data are from 1971–2021.
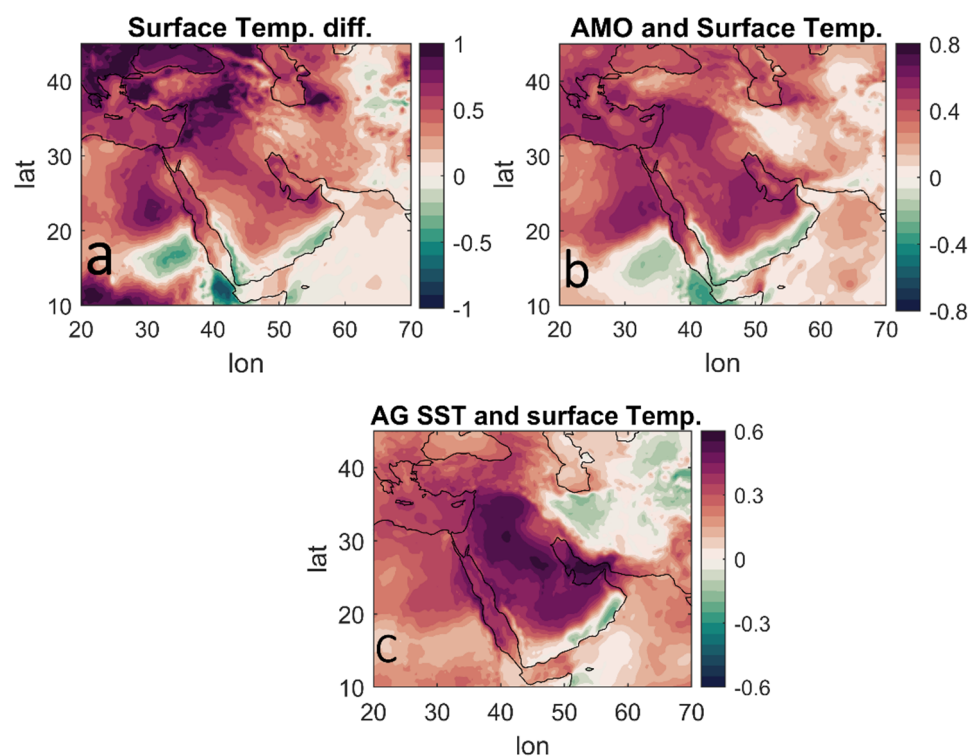

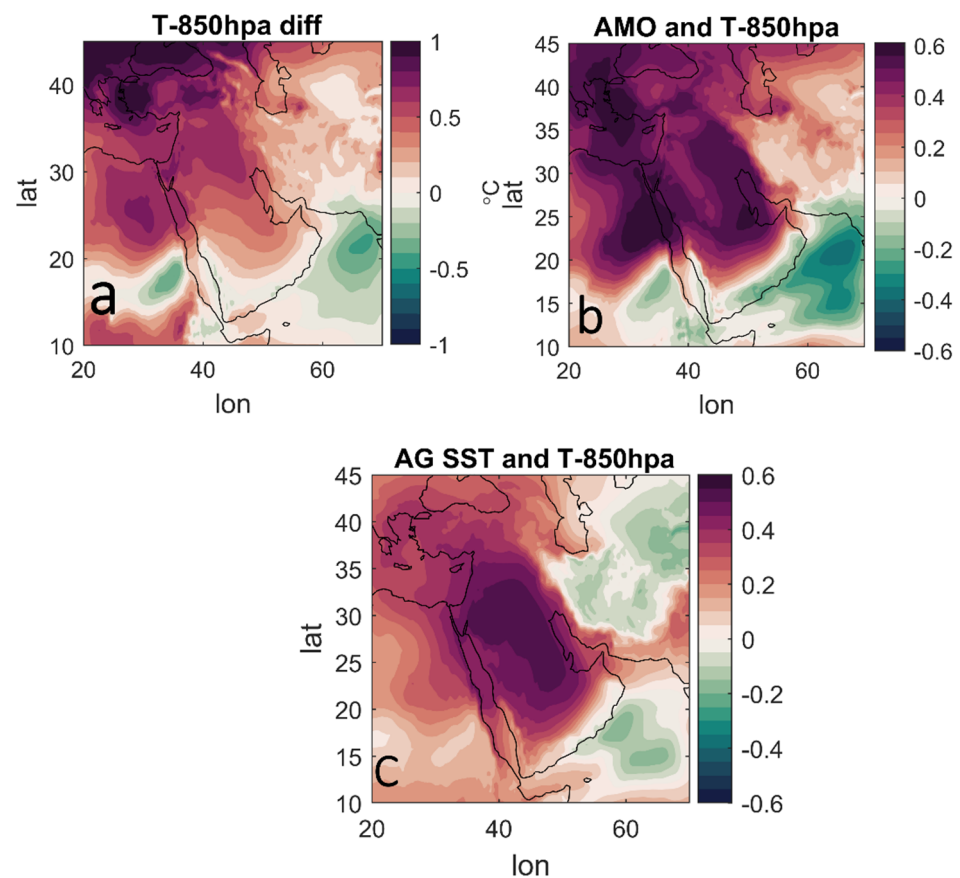**Figure 8.** Same as Figure 7, but for the surface temperate.

Figure 9. Same as Figure 7, but for upper-air temperate at 850 hpa.

Second, to investigate if the AMO plays any role in this change, a correlation analysis was conducted between the AMO and surface and 850 hpa temperature, and the results showed a similar pattern of temperature difference. Above a 0.6 positive correlation was observed over a wide part of AG countries, including the Northern AG, Northern Red Sea, and Eastern Mediterranean Sea (Figures 8b and 9b). Third, to investigate the indirect link with the AMO, the AGs SST time series was correlated with both temperature levels. Interestingly, the map looks similar to that shown in Figures 8a,b and 9a,b; a wide area of about 0.6 was observed over the Gulf countries.

This means that positive (negative) AMO events could cause the SST to increase (decrease) following the surrounding upper-air temperature. Thus, the AGs warming is related to the AMO over the North Atlantic Ocean, suggesting that the AMO signal could be transferred through the vertical temperature advection to the AGs SST.

4. Conclusions

Previous studies have documented that several ocean basins experienced significant SST warming behavior, including the AG, over the last few decades. Despite the potential wide-ranging impacts of this warming, less consideration has been given to what causes this warming over the AG and their driving forces. This paper investigates the impact of one of the possible large-scale atmospheric drivers, namely, the Atlantic multidecadal oscillation (AMO), which we hypothesize forces the AGs SST increase during the summer season. It was found that there was a significant spatial positive trend, with a maximum of up to 0.7 °C per decade, while the time series trend showed a significant shift after 1995, with an average value of about 0.36 °C per decade. It is important to mention that the global SST warming trend is about 0.11 °C per decade based on the 1980–2005 time average [4]. This means that the spatial and temporal trend in the AG is eight times and four times higher than the global value, respectively. Interestingly, the mid-90th shift concurs with the

phase shift of the AMO. Furthermore, strong relations were observed on both spatial and temporal scales, with a high pattern of a significant positive correlation coefficient between the AMO and SST.

The proposed underlying mechanisms that link the AMO with the AG decadal variability can be explained as follows: when the AMO is in a positive phase, surface northwesterly wind weakens, leading to (1) less advection of relatively cold air masses from Southern Europe to the AG and its surrounding area, (2) less evaporation and thus less surface cooling processes, and (3) thus the enhancement of the water masses stratification and the decrease in the upwelling process, and vice versa occurs for the negative phase. Further analyses are required to explore whether the impacts of the AMO are extended to other oceanic variables such as evaporation rate, heat transport, etc. Furthermore, the AMO seems to induce the significant warming of upper-air temperature over the AG and the surrounding area that covers the Arabian Peninsula, Northeast Africa, and a wide area over Southern Europe. These processes prove that the AMO is a possible candidate for the variability in the AGs SST during the summer season through the weakening of the Shamal wind, which is associated with an increasing upper-air temperature.

However, it is important to mention that the time series of the AGs SST does not always follow the same pattern as the AMO, especially during the period of 1930–1965, suggesting that the AGs SST derived by other large-scale climate modes during this period, and proving the information regarding the nonstationary characteristics in the relationship between the AGs SST and the AMO, can be documented in AG water. According to a previous study [36], special consideration should be provided to the role of East Asian winter monsoons and the Siberian anticyclone in the weakening of the AMO signal in the AG.

These findings help to bridge the gap between long-term climate variability and SST dynamics in the AG and to extend and support our recent growing knowledge by systematically understanding the trends and underlying climate mechanisms via remote atmospheric teleconnections, enabling a better evaluation of future climate scenarios for this important region.

References

1. Riegl, B.M.; Purkis, S.J.; Al-Cibahy, A.S.; Abdel-Moati, M.A.; Hoegh-Guldberg, O. Present Limits to Heat-Adaptability in Corals and Population-Level Responses to Climate Extremes. *PLoS ONE* **2011**, *6*, e24802. [CrossRef] [PubMed]
2. Meehl, G.A.; Washington, W.M.; Collins, W.D.; Arblaster, J.M.; Hu, A.; Buja, L.E.; Strand, W.G.; Teng, H. How Much More Global Warming and Sea Level Rise? *Science* **2005**, *307*, 1769–1772. [CrossRef] [PubMed]
3. Overland, J.E.; Alheit, J.; Bakun, A.; Hurrell, J.W.; Mackas, D.L.; Miller, A.J. Climate controls on marine ecosystems and fish populations. *J. Mar. Syst.* **2010**, *79*, 305–315. [CrossRef]
4. IPCC. *Climate Change 2013—The Physical Science Basis: Working Group I Contribution to the Fifth Assessment Report of the Intergovernmental Panel on Climate Change*; Cambridge University Press: Cambridge, UK, 2014. [CrossRef]
5. Collins, M.; Knutti, R.; Arblaster, J.; Dufresne, J.L.; Fichefet, T.; Friedlingstein, P.; Wehner, M. Long-term climate change: Projections, commitments and irreversibility. In *Climate Change 2013—The Physical Science Basis: Contribution of Working Group I to the Fifth Assessment Report of the Intergovernmental Panel on Climate Change*; Cambridge University Press: Cambridge, UK, 2013; pp. 1029–1136.
6. Belkin, I.M. Rapid warming of Large Marine Ecosystems. *Prog. Oceanogr.* **2009**, *81*, 207–213. [CrossRef]
7. Alosairi, Y.; Pokavanich, T. Seasonal circulation assessments of the Northern Arabian/Persian Gulf. *Mar. Pollut. Bull.* **2017**, *116*, 270–290. [CrossRef] [PubMed]
8. Bartlett, K.S. *Dust Storm Forecasting for Al Udeid AB, Qatar: An Empirical Analysis*; Air Force Inst of Tech Wright-Pattersonafb Oh School of Engineering: Dayton, OH, USA, 2004.
9. Hamidi, M.; Kavianpour, M.R.; Shao, Y. Synoptic analysis of dust storms in the Middle East. *Asia-Pac. J. Atmos. Sci.* **2013**, *49*, 279–286. [CrossRef]
10. Hamidi, M.; Kavianpour, M.R.; Shao, Y. Numerical simulation of dust events in the Middle East. *Aeolian Res.* **2014**, *13*, 59–70. [CrossRef]
11. Merlone, A.; Al-Dashti, H.; Faisal, N.; Cerveny, R.S.; AlSarmi, S.; Bessemoulin, P.; Krahenbuhl, D. Temperature extreme records: World Meteorological Organization metrological and meteorological evaluation of the 54.0 C observations in Mitribah, Kuwait and Turbat, Pakistan in 2016/2017. *Int. J. Climatol.* **2019**, *39*, 5154–5169. [CrossRef]
12. Shaltout, M. Recent sea surface temperature trends and future scenarios for the Red Sea. *Oceanologia* **2019**, *61*, 484–504. [CrossRef]
13. Bargahi, H.R.; Shokri, M.R.; Kaymaram, F.; Fatemi, M.R. Changes in reef fish assemblages following multiple bleaching events in the world's warmest sea (Kish Island, the Persian Gulf). *Coral Reefs* **2020**, *39*, 603–624. [CrossRef]
14. Brandl, S.J.; Johansen, J.L.; Casey, J.M.; Tornabene, L.; Morais, R.A.; Burt, J.A. Extreme environmental conditions reduce coral reef fish biodiversity and productivity. *Nat. Commun.* **2020**, *11*, 3832. [CrossRef] [PubMed]
15. Al-Subhi, A.M. A comprehensive statistical analysis of nearly 35 years AVHRR SST data from the Arabian Gulf: Trends, anomalies, and intra-inter-annual seasonality. *JKAU Mar. Sci.* **2019**, *29*, 53–72. [CrossRef]
16. Al-Rashidi, T.B.; El-Gamily, H.I.; Amos, C.L.; Rakha, K.A. Sea surface temperature trends in Kuwait bay, Arabian Gulf. *Nat. Hazards* **2009**, *50*, 73–82. [CrossRef]
17. Shirvani, A.; Nazemosadat, S.M.J.; Kahya, E. Analyses of the Persian Gulf sea surface temperature: Prediction and detection of climate change signals. *Arab. J. Geosci.* **2015**, *8*, 2121–2130. [CrossRef]
18. Shirvani, A. Change point detection of the Persian Gulf sea surface temperature. *Theor. Appl. Clim.* **2017**, *127*, 123–127. [CrossRef]
19. Alosairi, Y.; Alsulaiman, N.; Rashed, A.; Al-Houti, D. World record extreme sea surface temperatures in the northwestern Arabian/Persian Gulf verified by in situ measurements. *Mar. Pollut. Bull.* **2020**, *161*, 111766. [CrossRef] [PubMed]
20. Burt, J.A.; Paparella, F.; Al-Mansoori, N.; Al-Mansoori, A.; Al-Jailani, H. Causes and consequences of the 2017 coral bleaching event in the southern Persian/Arabian Gulf. *Coral Reefs* **2019**, *38*, 567–589. [CrossRef]
21. Purkis, S.J.; Riegl, B. Spatial and temporal dynamics of Arabian Gulf coral assemblages quantified from remote-sensing and in situ monitoring data. *Mar. Ecol. Prog. Ser.* **2005**, *287*, 99–113. [CrossRef]
22. Sheppard, C.; Loughland, R. Coral mortality and recovery in response to increasing temperature in the southern Arabian Gulf. *Aquat. Ecosyst. Health Manag.* **2002**, *5*, 395–402. [CrossRef]
23. Riegl, B. Effects of the 1996 and 1998 positive sea-surface temperature anomalies on corals, coral diseases and fish in the Arabian Gulf (Dubai, UAE). *Mar. Biol.* **2002**, *140*, 29–40.
24. Krokos, G.; Papadopoulos, V.P.; Sofianos, S.S.; Ombao, H.; Dybczak, P.; Hoteit, I. Natural Climate Oscillations may Counteract Red Sea Warming Over the Coming Decades. *Geophys. Res. Lett.* **2019**, *46*, 3454–3461. [CrossRef]
25. Alawad, K.A.; Al-Subhi, A.M.; Alsaafani, M.A.; Alraddadi, T.M. Decadal variability and recent summer warming amplification of the sea surface temperature in the Red Sea. *PLoS ONE* **2020**, *15*, e0237436. [CrossRef]
26. Ehsan, M.A.; Nicolì, D.; Kucharski, F.; Almazroui, M.; Tippett, M.K.; Bellucci, A.; Ruggieri, P.; Kang, I.-S. Atlantic Ocean influence on Middle East summer surface air temperature. *NPJ Clim. Atmos. Sci.* **2020**, *3*, 5. [CrossRef]
27. Al Senafi, F. Atmosphere-Ocean Coupled Variability in the Arabian/Persian Gulf. *Front. Mar. Sci.* **2022**, *9*, 192. [CrossRef]

28. Rayner, N.A.; Parker, D.E.; Horton, E.B.; Folland, C.K.; Alexander, L.V.; Rowell, D.P.; Kent, E.C.; Kaplan, A. Global analyses of sea surface temperature, sea ice, and night marine air temperature since the late nineteenth century. *J. Geophys. Res.* **2003**, *108*, 4407. [CrossRef]

29. Reynolds, R.W.; Smith, T.M.; Liu, C.; Chelton, D.B.; Casey, K.S.; Schlax, M.G. Daily High-Resolution-Blended Analyses for Sea Surface Temperature. *J. Clim.* **2007**, *20*, 5473–5496. [CrossRef]

30. Enfield, D.B.; Mestas-Nuñez, A.M.; Trimble, P.J. The Atlantic Multidecadal Oscillation and its relation to rainfall and river flows in the continental U.S. *Geophys. Res. Lett.* **2001**, *28*, 2077–2080. [CrossRef]

31. Mann, H.B. Nonparametric tests against trend. *Econom. J. Econom. Soc.* **1945**, *13*, 245–259. [CrossRef]

32. Kendall, M.G. *Rank Correlation Methods*, 3rd ed.; Hafner Publishing Company: New York, NY, USA, 1962.

33. Zhang, W.; Mei, X.; Geng, X.; Turner, A.G.; Jin, F.F. A nonstationary ENSO–NAO relationship due to AMO modulation. *J. Clim.* **2019**, *32*, 33–43. [CrossRef]

34. Nakamura, N.; Kayanne, H.; Iijima, H.; McClanahan, T.R.; Behera, S.K.; Yamagata, T. Mode shift in the Indian Ocean climate under global warming stress. *Geophys. Res. Lett.* **2009**, *36*. [CrossRef]

35. Timm, O.; Pfeiffer, M.; Dullo, W. Nonstationary ENSO-precipitation teleconnection over the equatorial Indian Ocean documented in a coral from the Chagos Archipelago. *Geophys. Res. Lett.* **2005**, *32*. [CrossRef]

36. Ionita, M.; Felis, T.; Lohmann, G.; Rimbu, N.; Pätzold, J. Distinct modes of East Asian Winter Monsoon documented by a southern Red Sea coral record. *J. Geophys. Res. Oceans* **2014**, *119*, 1517–1533. [CrossRef]

37. Alawad, K.; Al-Subhi, A.; Alsaafani, M.; Alraddadi, T. Atmospheric Forcing of the High and Low Extremes in the Sea Surface Temperature over the Red Sea and Associated Chlorophyll-a Concentration. *Remote. Sens.* **2020**, *12*, 2227. [CrossRef]

38. Miyazaki, H. Evaluation of Heat Island Intensity for Coastal Urban Areas. *J. Heat Isl. Inst. Int.* **2012**, *7*, 255–262.

39. Shaltout, M.; Omstedt, A. Recent sea surface temperature trends and future scenarios for the Mediterranean Sea. *Oceanologia* **2014**, *56*, 411–443. [CrossRef]

40. Hong, X.; Lu, R.; Li, S. Amplified summer warming in Europe–West Asia and Northeast Asia after the mid-1990s. *Environ. Res. Lett.* **2017**, *12*, 094007. [CrossRef]

41. Hong, X.; Lu, R. The meridional displacement of the summer Asian jet, Silk Road Pattern, and tropical SST anomalies. *J. Clim.* **2016**, *29*, 3753–3766. [CrossRef]

42. Sun, X.; Li, S.; Hong, X.; Lu, R. Simulated Influence of the Atlantic Multidecadal Oscillation on Summer Eurasian Nonuniform Warming since the Mid-1990s. *Adv. Atmos. Sci.* **2019**, *36*, 811–822. [CrossRef]

43. Hu, P.; Chen, W.; Chen, S.; Liu, Y.; Wang, L.; Huang, R. Impact of the September Silk Road Pattern on the South China Sea summer monsoon withdrawal. *Int. J. Clim.* **2020**, *40*, 6361–6368. [CrossRef]

44. Yu, Y.; Notaro, M.; Kalashnikova, O.V.; Garay, M.J. Climatology of summer Shamal wind in the Middle East. *J. Geophys. Res. Atmos.* **2016**, *121*, 289–305. [CrossRef]

45. Wang, C.; Weisberg, R.H.; Yang, H. Effects of the wind speed–evaporation–SST feedback on the El Niño–Southern Oscillation. *J. Atmos. Sci.* **1999**, *56*, 1391–1403.